Electrocatal (2010) 1:95–103
DOI 10.1007/s12678-010-0010-5

Synthesis and Characterization of Ordered Intermetallic Nanostructured PtSn/C and PtSb/C and Evaluation as Electrodes for Alcohol Oxidation

Marcelo Rodrigues da Silva · Antonio Carlos Dias Ângelo

Published online: 17 March 2010

Abstract Ordered intermetallic compounds of Pt-based metal electrocatalysts have been recently proposed as very efficient anode materials for reactions involved in low temperature fuel cells. In this work, supported ordered intermetallics nanoparticles PtSn/C and PtSb/C and supported platinum nanoparticles (Pt/C) were prepared at low temperature from their metallic precursors by a modified polyol process, using tetraethylene glycol as the solvent and reducing agent and Vulcan carbon XC-72 as the support. Powder X-ray diffraction patterns confirmed the presence of the ordered intermetallic phase and furnished lattice parameters and crystal structure. Transmission electron microscopy images show that the metal particles were highly dispersed and distributed homogeneously over the support, and energy-dispersive X-ray spectroscopy showed that the composition of the final product is within that of the desired stoichiometry. The electrocatalytic activity of these intermetallic phases toward the oxidation of methanol, ethanol, and ethylene glycol were confirmed by cyclic voltammetry and steady-state polarization curve at room temperature. The results showed that the supported intermetallic nanoparticles PtSn and PtSb are more active than the Pt/C catalyst prepared by the same method for alcohol oxidation.

Keywords Ordered intermetallic phase · Nanoparticles · Polyol · Electrocatalytic activity

M. Rodrigues da Silva · A. C. D. Ângelo (✉)
Laboratório de Eletrocatálise, Departamento de Química,
Faculdade de Ciências, UNESP,
Bauru, SP, P.O. Box 473, 17033-360, Brazil
e-mail: acangelo@fc.unesp.br

Introduction

In recent years, an enormous number of electrode materials have been investigated in the search for electrocatalytic activity. Among the many electrochemical systems that incorporate electrocatalysis, fuel cells have a uniquely high profile as they are intimately related to the improvement of systems to generate energy [1].

One of the greatest challenges facing electrocatalysis is without doubt in the synthesis of the catalytic material, since the relative performance of a given sample depends closely on the synthetic procedure followed. Currently, Pt-based metal alloys are the materials most often used in fuel cells, since this composition not only minimizes the cost of the device by diminishing the load of Pt, but also reduces the susceptibility of the platinum to the poisoning by intermediates and by-products of oxidation of the organic fuels [2, 3].

In real fuel cell systems, electrocatalytic materials have to be synthesized on the nanometric scale, as nanostructured material offers a much larger active surface than a bulk electrode and supports higher current densities. Owing to their extremely small dimensions, nanometric structures are characterized by a large volume fraction of grain boundaries or interfaces, which can alter greatly the range of physical and chemical properties, relative to those seen in the normal crystalline material [4, 5].

Although the metal alloys generally make efficient electrocatalytic materials, they tend to exhibit low physicochemical stability, as well as an inhomogeneous crystal structure in the bulk of the material [6, 7]. As a consequence, it is difficult to get a deep understanding of the electrocatalytic process [8].

From this context, ordered intermetallic phase compounds emerged as an alternative to the conventional metal

alloys [9]. The intermetallics are a special class of metal alloys that offer unique features across a broad range of techniques and application. They are formed out of two or more metallic elements, usually transition metals, which combine in simple stoichiometric proportions within certain narrow composition ranges, giving rise to a crystal structure different from those of the original metals [10]. This geometric change in the structure provokes an altered electron distribution among the atoms of the intermetallic compound formed. Another important feature is the homogeneity of the crystal structure throughout the material, making these compounds especially interesting for the study of electrochemical processes that take place on the surface during the oxidation of organic fuels and hydrogen [11, 12]. More recently, Innocente and Ângelo reported the use of Pt-based ordered intermetallic compounds (PtSn and PtSb) as promising anodic materials for the hydrogen oxidation reaction. Acting as anode, these materials have showed higher current densities than commercial pure Pt, as well as being lower susceptibility to the surface blocking by CO molecules [13, 14]. Zhang and Xia studied the electrocatalytic activity of ordered intermetallic PtSb for methanol electro-oxidation. The results showed that the intermetallic was catalytically more active than pure platinum by considering the onset potential and current density parameters [8]. Bauer and coworkers have investigated the use of PtPb intermetallic supported on carbon for formic acid electro-oxidation. The intermetallic PtPb was shown to be more active than Pt/Vulcan (E-TEK) and PtRu/Vulcan (E-TEK) regarding the current density and onset potential [15]. In spite of these published papers, the use of the nanostructured ordered intermetallic compounds in the electrocatalysis of the organic fuel reactions is still very limited, as evidenced by the low number of studies reported in the literature. To the best of our knowledge, there are no published papers that report the use of Pt-based nanostructured ordered intermetallic compounds as "active" materials for the electro-oxidation of more complex alcohols than methanol.

The polyol process is an efficient way of preparing bimetallic nanoparticles in the form of alloys [16, 17] or ordered intermetallic compounds [18–22] at low temperature. In this method, the nanostructures are formed in suspension within the solution, ensuring stability and control of particle size [23]. Roychowdhury and coworkers synthesized polycrystalline nanoparticles of ordered PtBi intermetallic phases by the polyol process. Catalysis of the oxidation of formic acid by the particles was then studied by cyclic voltammetry, revealing that the PtBi nanoparticles had better electrocatalytic activity than Pt or PtRu nanoparticles [18]. Cable and Schaak synthesized PtSb and PtSn intermetallic nanocrystals by means of a modified polyol method, with tetraethylene glycol as solvent and at a high temperature, around 200°C and 230°C, respectively, in highly reducing conditions provided by sodium borohydride ($NaBH_4$). In this case, however, no electrochemical tests were done to investigate the electrocatalytic activity of the intermetallic nanocrystals [19].

In this context, the aim of this paper is to present a preliminary electrochemical evaluation of PtSb/C and PtSn/C intermetallic nanoparticles as active material for methanol, ethanol, and ethylene glycol oxidation reactions in an acidic medium.

Experimental

Synthesis of the Nanostructured Materials

The supported intermetallic electrocatalysts (PtSn/C and PtSb/C) and supported platinum (Pt/C) were prepared in the proportion of 20:80 (*w*/*w*) metal:carbon support (Vulcan XC-72), by a procedure based on that described by Roychowdhury and coworkers [18]. Firstly, 50 mL tetraethylene glycol (TEG; Merck, p.a.) and 400 mg of finely powdered carbon (Vulcan XC-72) were mixed in a beaker, which was placed in an ultrasonic bath for 40 min in an inert atmosphere (N_2, White Martins 5.0), to disperse the support in the solvent. Next, 71.91 mg $SnCl_2.2H_2O$ (Mallinckrodt) or 72.01 mg $SbCl_3$ (Sigma-Aldrich) was added to the mixture and 500 μL of the Triton X-100 (d=1.029 gcm^{-3}; Sigma-Aldrich) as a stabilizer. The whole mixture was transferred to a round-bottomed flask with three necks, which was coupled to a vertical bulb reflux condenser and heated to 210°C by a heating jacket, remaining under reflux at this temperature for 16 h, to complete the first synthetic step. In another vessel, 50 mL TEG was purged with N_2 gas (White Martins, 5.0) for 40 min. A weighed quantity of hexachloroplatinic (IV) acid ($H_2PtCl_6.6H_2O$; Sigma-Aldrich), stoichiometric with the Sn or Sb precursor, was dissolved in the deaerated solvent, giving an orange solution. At the end of the first step, this second metal precursor was added dropwise from a micropipette through a side-neck to the partially reduced Sn or Sb precursor, over a period of 1 h. The reflux continued at 250°C for a further 48 h, giving a total of 67 h for the whole synthesis. The ordered intermetallic nanoparticles were synthesized in three steps. The first was the partial reduction of tin, Sn^{2+}/Sn^{o} (E^{o}_{red}=−0.14 V), or antimony, Sb^{3+}/Sb^{o} (E^{o}_{red}=+0.15 V), by TEG (bp=314°C) acting as both solvent and reducing agent. The ease of reduction of the metal precursors used to synthesize the catalysts is related to the reduction potential (E^{o}_{red}) of the oxidized metal. The reduction of the couple Pt^{4+}/Pt^{o} (E^{o}_{red}=+1.3 V) is thermodynamically much more favorable than reduction of the tin or antimony precursors, as their reduction potentials are less positive. Therefore, in the second step, the chloroplatinic

acid was added to the already partially reduced tin or antimony, so that the metallic Pt formed initially would catalyze their further reduction. When the tin or antimony precursor was added after partial reduction of the platinum, the final product consisted entirely of a face-centered cubic (fcc) phase of platinum [18]. The third step was the formation of the ordered intermetallic phase. The bimetallic particles grow on the carbon support as a disordered alloy, and the metal atoms then slowly rearrange themselves into the stable ordered intermetallic phase [15, 19, 21]. Thus, an extra 48 h of heating was needed, to allow this atomic diffusion to go to completion.

For the purpose of comparing the electrochemical test results for the intermetallic particles with a standard material in the same state, supported platinum (Pt/C) was synthesized by a method similar to the first step described above, but with the precursor $H_2PtCl_6.6H_2O$. The Pt/C nanoparticles were formed in just 4 h of refluxing at 100°C. The final product, a black powder, was washed several times with acetone, to remove all traces of organic material (both solvent molecules and those produced by oxidation of the solvent) adsorbed on the surface of the particles, and then several times with deionized water. The powder was then dried in an oven at 80°C for 24 h.

Physical Characterization

The synthesized materials were characterized by powder X-ray diffraction spectroscopy (pXRD), with a Rigaku RINT 2000 diffractometer equipped with a Cu–$K\alpha_1$ radiation source, to identify the ordered intermetallic phase. The spectra were recorded as a mean of three scans, at a rate of 1º min^{-1}, from 2θ=20º to 80º. The morphology, distribution, and size of the intermetallic nanoparticles were observed with a JEOL transmission electron microscope (TEM), model JEM-1200 EX II, and the atomic surface composition of the product was estimated by energy-dispersive X-ray spectroscopy (EDX) in a LEO-440 electron microscope with an Oxford 7060 EDS detector, at a resolution of 113 eV.

Electrochemical Evaluation

The electrochemical activity of the materials for the oxidation of methanol, ethanol, and ethylene glycol (Merck, p.a.) was tested by cyclic voltammetry and steady-state polarization curves, using an ultrathin layer electrode. The ultrathin layer-working electrode was fashioned from a vitreous carbon disk (geometric area of cross section 0.031 cm^2), previously polished with 0.1 and 0.05 μm alumina. A suspension was prepared by mixing 6 mg of catalyst powder, 200 μL of Nafion (5.5% by weight), 200 μL of isopropyl alcohol, and 100 μL deionized water and agitating the mixture in an ultrasonic bath for 1 h. As usually employed in similar studies, the specific activity of each electrode was achieved taking into account the amount of Pt on the surface of the electrode. An aliquot of 10 μL of this suspension was applied to the surface of the vitreous carbon disk and allowed to dry for 24 h in a desiccator. The electrochemical measurements were carried out at room temperature in electrolytic solutions of 0.15 mol L^{-1} $HClO_4$ (Merck, 70%), or 0.15 mol L^{-1} methanol, ethanol, or ethylene glycol (Merck, p.a.) plus 0.15 mol L^{-1} $HClO_4$, purged with nitrogen gas (White Martins, 5.0). The data were obtained by using an EG&G PAR283 potentiostat/galvanostat, controlled by M270 software. For this, it was employed a two-compartment glass cell. The reversible hydrogen electrode (RHE) was employed as reference system and a large surface area platinum wire as counter electrode. The voltammograms shown in the electrochemical characterization of the catalysts represent the recording of the 100th cycle, while those shown in the evaluation of the material as an anode for the oxidation of the organic fuels refer to the 20th cycle. It was verified that the number of cycles performed was large enough to establish the steady-state voltammetric profile, as the current did not show noticeable change between the first and last cycles. Steady-state data were obtained in the same experimental setup in a chronoamperometric way by registering the steady-state current after 300 s of applied potential. For comparison of the electrochemical performance of the electrode materials, it was determined the onset potential (OP, estimated as the potential concerned to the first current of the raising faradaic curve for the alcohol oxidation) and the maximum specific current reached for the alcohol oxidation on the electrode material per amount of platinum on the surface (j_p, $mA.mg_{Pt}^{-1}$).

Results and Discussion

The powder diffractograms of the final products are seen in Fig. 1. The diffraction peaks were compared with literature data (PCPDFWin, version 2.4, JCODS—ICDD). The PtSn and PtSb supported intermetallics materials showed a first peak at about 2θ=24.7°, representing the diffraction from plane (100). However, this peak may be superimposed on the low intensity, broad peak of the Vulcan carbon support, which is typically seen in materials supported on carbon [24]. In the case of Pt/C, this low intensity peak certainly refers to the support, since the first diffraction plane for fcc platinum appears at around 2θ=39.6°. The PtSn/C nanoparticles produced diffraction peaks at 2θ=30.1°, 41.7°, 44.1°, 51.2°, 54.6°, 57.1°, 62.3°, 74.6°, and 79.3°, assigned to reflections from the (101), (102), (110), (200), (201),

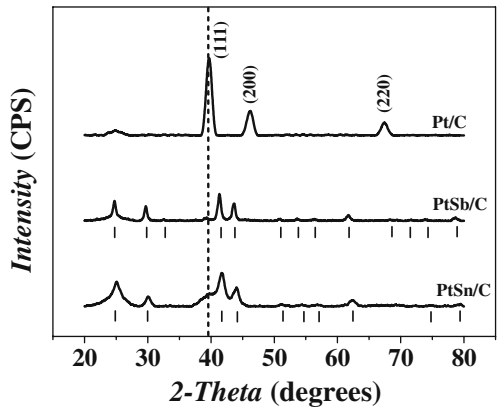

Fig. 1 Diffractograms of the nanostructured intermetallics materials and Pt/C

(112), (202), (203), and (212) planes of the ordered intermetallic phase PtSn (PDF card no. 25-0614) [19, 21]. Turning to the diffractograms of the PtSb/C nanoparticles, the most intense peaks at 2θ=29.8°, 32.7°, 41.3°, 43.6°, 50.8°, 53.6°, 56.4°, 61.6°, 68.5°, 71.3°, 74.1°, and 78.8°, ascribed to the (101), (002), (102), (110), (200), (201), (103), (202), (004), (211), (104), and (202) planes, correspond to an ordered intermetallic phase PtSb (PDF card no. 72-1440) [22]. The ordered intermetallics phases PtSn (a=4.100 Å, c=5.432 Å) and PtSb (a=4.130 Å, c=5.472 Å) nanoparticles belong to the crystallographic hexagonal system ($P6_3/mmc$ (194)). The Pt/C synthesized by the same method that the intermetallics (first step, in 4 h at 100°C) is identified as belonging to the fcc cubic system (Fm3m (225)) with a=3.923 Å (PDF card no. 04-0802). The presence of a phase of free Pt, both in PtSn/C and PtSb/C (peaks at 2θ=39.8°, 46.2°, and 67.5°, corresponding to the planes (111), (102), and (220), respectively), may be connected with the high reduction potential of the Pt^{+4}/Pt^0 couple, compared to that of Sb^{+3}/Sb^0 or Sn^{+2}/Sn^0. During the synthesis, some Pt^0 particles may have been formed very rapidly and become stable, so that they did not interact with the metallic tin or antimony produced later, to form the intermetallic phase. Such phenomenon has been early reported from similar synthesis of the ordered intermetallic compounds [8, 18] and Pt-based metal alloys [25–27]. Despite this evidence of a second phase, the phase PtSn and PtSb is seen to predominate in the final product.

An estimate of the mean size of the metal particles dispersed in the larger particles of carbon was obtained by means of the Scherrer equation [28]. The mean particle diameters found in this way were around 3 and 7 nm for PtSn and PtSb, respectively, and 7.4 nm for Pt synthesized by the same method.

TEM images (Fig. 2) show that the metal particles in PtSn/C, PtSb/C, and Pt/C were highly dispersed and distributed homogeneously over the Vulcan carbon support. The histogram distribution, which was obtained by directly measuring the size of a number of 100 (PtSn and Pt) and 60 (PtSb) randomly selected metal particles in the magnified TEM image, showed that the intermetallic PtSn particles were smaller than those of PtSb and Pt. Comparing the particle sizes estimated by TEM and XRD, it is seen in Table 1 that the two sets of results are remarkably similar.

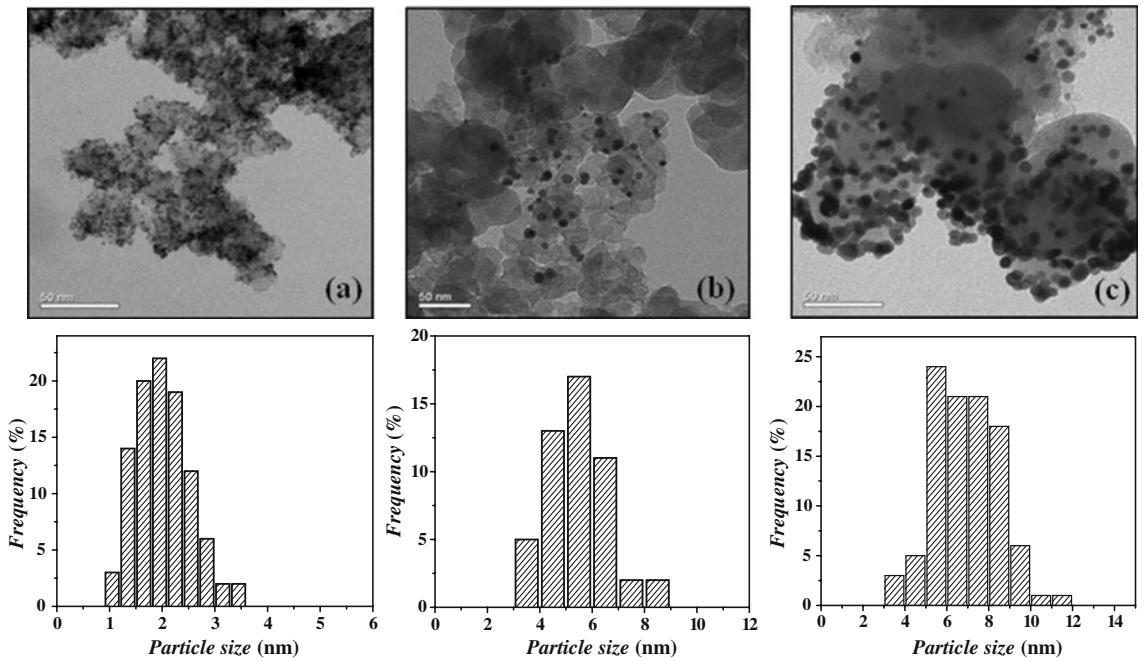

Fig. 2 TEM image of the supported **a** PtSn/C, **b** PtSb/C, and **c** Pt/C materials and the corresponding particle size distribution histogram

Table 1 Mean diameters (XRD and TEM) and atomic compositions (EDX analysis) of metal nanoparticles of materials prepared by the polyol method

Materials	Mean particle diameter (nm)		Mean atomic fraction±standard deviation (%)		
	XRD	TEM	Pt	Sb	Sn
PtSb/C	7	5.5	45.9±0.7	54.1±0.7	–
PtSn/C	3.0	2	49.5±2.3	–	50.53±2.3
Pt/C	7.4	7	–	–	–

EDX was used at five randomly located points on each sample to analyze qualitatively the elemental composition of the material and to calculate the mean atomic fraction of each element found. The results are given in Table 1, and they prove that the polyol method was suitable for the production of intermetallic nanoparticles in the required stoichiometry (1:1), within acceptable limits.

The voltammetric profile of the supported intermetallics nanoparticles PtSn and PtSb and the Pt/C in perchloric acid medium are shown in Fig. 3. During electrochemical testing, all the electrode materials proved electrochemically stable under the conditions of potential cycling used, with little current variation from the first to the last (100th) cycle. Note that the hydrogen adsorption and desorption regions, between 50 and 400 mV, are not well defined. This is typical of platinum-based metal alloys supported on carbon (PtM/C) and platinum supported on carbon (Pt/C) [29, 30]. The formation of oxygenated species starts around 650 mV (relative to the RHE) on the surface of the Pt/C catalysts, whereas on PtSb/C and PtSn/C, this hydroxide region begins at about 400 mV, which corresponds to a shift of the OP to a value about 250 mV less positive than Pt/C material under the same experimental conditions. The formation of these species at less positive potentials on the catalytic surface is desirable, so that, subsequently, the CO (formed as an intermediate in the oxidation of organic fuels) can be oxidized more readily, releasing active sites on the catalyst [31, 32]. Nevertheless, other characteristics can also strongly influence on the electrochemical performance of the electrode material toward the alcohol oxidation reaction.

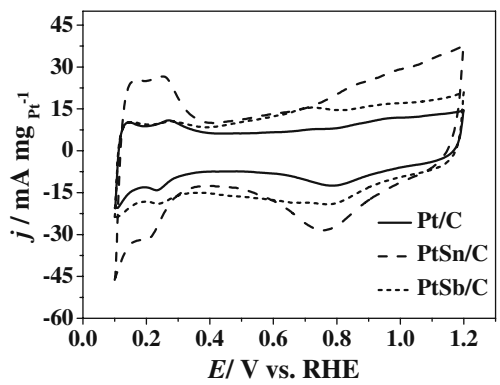

Fig. 3 Voltammetric profile of the PtSn/C and PtSb/C intermetallics and Pt/C in 0.15 mol L^{-1} perchloric acid solution. v=50 mV s^{-1}

Figure 4a illustrates the cyclic voltammograms, and Fig. 5a illustrates the steady-state polarization curves recorded with the intermetallic and platinum electrodes during the electro-oxidation of methanol. It can be seen in the voltammetric profiles that processes similar to those that occur on the surface of the Pt/C electrode are also observed on the intermetallic PtSn/C and PtSb/C. This behavior has been reported by others on polycrystalline Pt [33], PtSb intermetallic [8] and PtSn alloys [24], both of which exhibit two oxidation peaks, one in the anodic sweep and the other in the reverse sweep. The peak observed in the anodic sweep is attributed to the oxidation of methanol, while that one in the reverse sweep corresponds to the oxidation of molecular fragments arising from the rupture of the methanol molecule (carbonaceous residues), which are adsorbed on the electrode surface [8, 34]. The electrochemical performance of the intermetallic electrodes for the electro-oxidation of methanol was assessed by determining the maximum oxidation current density (j_p) and OP as earlier defined. These parameters, for the reaction on PtSn/C and PtSb/C, are compared with those for carbon-supported platinum (Pt/C), in Tables 2 and 3. From the results, it is clear that the PtSn/C electrode was by far the most active material for methanol oxidation, with a maximum oxidation current density (142 and 66 mA/mg_{Pt}) greater than that of PtSb/C (115 and 33 mA/mg_{Pt}) and Pt/C (56 and 20 mA/mg_{Pt}), whose data were obtained by cyclic voltammetry and steady-state measurements, respectively. The OP values determined for the reaction on intermetallic PtSn/C was 60 and 130 mV (from potentiodynamic measurements), and 90 and 150 mV (from steady-state measurements) less positive than PtSb/C and Pt/C, respectively, that confirm the lower energy required to start the oxidation of the methanol molecule on that surface as compared to the other electrode materials.

Cyclic voltammograms and steady-state polarization curves for the electro-oxidation of ethanol are shown in Figs. 4b and 5b, respectively. For the oxidation of ethanol on a polycrystalline Pt surface, two well-known processes appear, characterized by two oxidation peaks, one in the anodic and the other in the reverse sweep [35–38]. Processes similar to those described for polycrystalline Pt were registered for the ethanol oxidation reaction on the surfaces of the intermetallics PtSn/C and PtSb/C, and Pt/C. Both the intermetallic catalysts produce a peak very

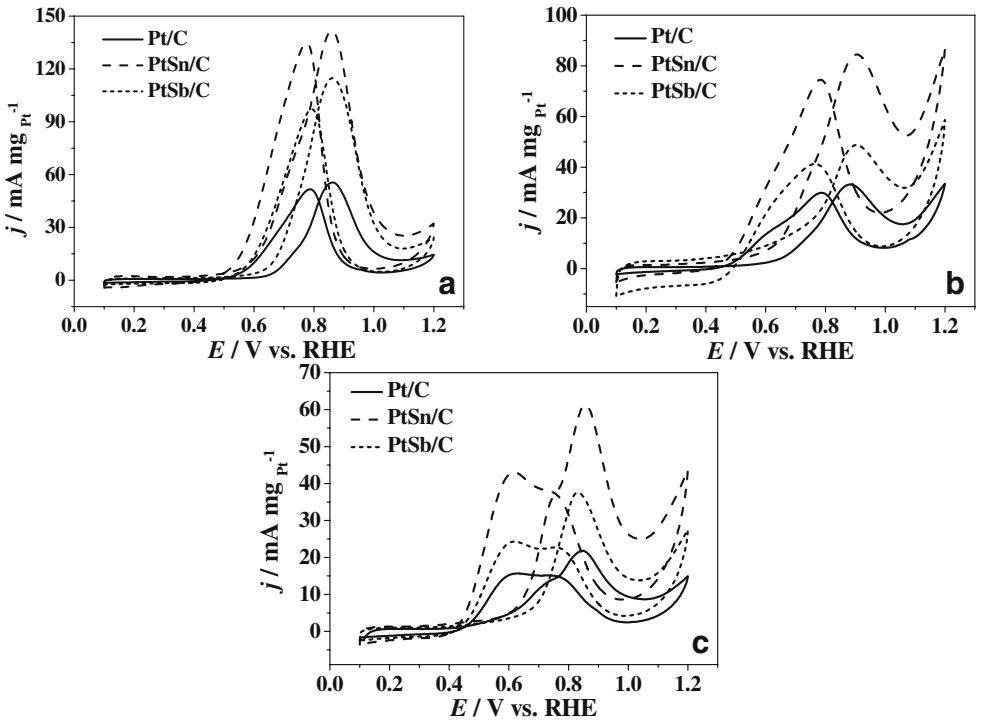

Fig. 4 Cyclic voltammograms of PtSn/C and PtSb/C intermetallics and Pt/C electrodes in 0.15 mol L^{-1} $HClO_4$ solutions containing: **a** 0.15 mol L^{-1} methanol, **b** 0.15 mol L^{-1} ethanol, **c** 0.15 mol L^{-1} ethylene glycol. v=20 mV s^{-1}

pronounced of electro-oxidation of ethanol in the anodic sweep. In the reverse sweep, the materials show a characteristic oxidation peak at around 800 mV. This may be related to the oxidation of fragments of ethanol molecules broken down during the anodic sweep as previously reported [39, 40]. Regarding the electro-oxidation of ethanol, the voltammograms obtained for the reaction on the intermetallics PtSn/C and PtSb/C showed onset potentials that were 170 and 230 mV less positive, respectively, than the same parameter measured for the reaction taking place on Pt/C. From steady-state polarization measurements, it was observed that the use of

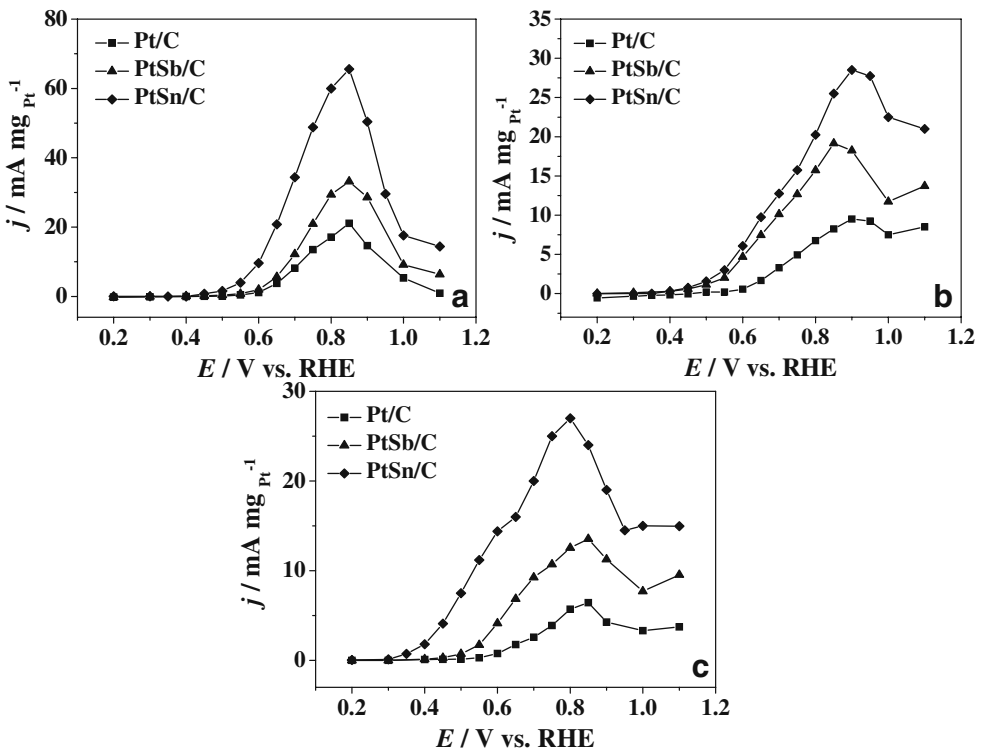

Fig. 5 Steady-state polarization curves for the alcohol oxidation on PtSn/C and PtSb/C intermetallics and Pt/C electrodes in 0.15 mol L^{-1} $HClO_4$ solutions containing: **a** 0.15 mol L^{-1} methanol, **b** 0.15 mol L^{-1} ethanol, **c** 0.15 mol L^{-1} ethylene glycol

Table 2 Electrochemical performances of the nanostructured materials in the electro-oxidation of methanol, ethanol, and ethylene glycol by cyclic voltammetry in perchloric acid solution

Catalysts	Organic fuel					
	Methanol		Ethanol		Ethylene glycol	
	j_p (mA.mgPt^{-1})	OP (mV)	j_p (mA.mgPt^{-1})	OP (mV)	j_p (mA.mgPt^{-1})	OP (mV)
Pt/C	56	670	33	670	22	650
PtSn/C	142	540	85	500	62	600
PtSb/C	115	600	49	440	38	600

intermetallics PtSn/C and PtSb/C as anode for the ethanol oxidation reaction has provoked a displacement of the OP to values about 150 mV less positive than the value obtained as Pt/C was employed as electrode material. The same qualitative performance already mentioned for the methanol oxidation reaction was also obtained in the ethanol oxidation reaction, i.e., PtSn/C electrode material has presented the highest value of current density as compared to PtSb/C and Pt/C materials. The data concerned to such performance are also joined in Tables 2 and 3.

The cyclic voltammograms and steady-state polarization curves produced with the three nanostructured electrode materials in the presence of ethylene glycol are illustrated in Figs. 4c and 5c, respectively. The processes involved in the electro-oxidation of ethylene glycol on the surface of polycrystalline Pt by means of cyclic voltammetry are less well understood than in the cases of methanol and ethanol oxidation [41]. All of the carbon-supported materials show a pronounced oxidation peak in the anodic sweep. It is thought that the two oxidation peaks that appear in the cathodic sweep, with all the electrode materials, as seen in the electro-oxidation of ethanol, arise from the oxidation of fragments left by the rupture of the ethylene glycol molecule during the anodic sweep, which remain on the electrode surface. This double peak was noticed in the paper of Wang and coworkers for the ethylene glycol oxidation reaction on platinum [42], where the authors suggested that the first peak in the cathodic sweep is mainly related to the oxidation of CO_{ad} species, which were produced in the low-potential region of that forward scan or in the preceding negative-going scans, and the second peak is attributed to ethylene glycol oxidation to incompletely oxidized C_2 compounds. Chatterjee and coworkers studying the electro-oxidation of ethylene glycol in the Pt- and PtRu-supported materials reported only one oxidation peak in the anodic scan and another one in the reverse scan [43]. Selvaraj and coworkers have also observed the same behavior on Pt and PtRu nanoparticles-modified multiwalled carbon nanotubes. The authors suggested that the oxidation peak in the anodic sweep corresponds to the oxidation of ethylene glycol, and the reductive peak in the reverse scan is due to the reduction of Pt oxide [44]. As it can be clearly seen, any agreement on the explanation for the electrochemical processes observed for the ethylene glycol oxidation reaction is far to be achieved, and more detailed and deeper studies are urgently demanded and are being developed in our research group. As it was previously found for methanol and ethanol electro-oxidation, the nanostructured intermetallics PtSn/C and PtSb/C show higher electrochemical activity for the ethylene glycol oxidation reaction than platinum under the same experimental conditions. The data concerned to such performance are joined in Tables 2 and 3.

We proposed that this better performance of nanostructured intermetallics compounds PtSn/C and PtSb/C in the electro-oxidation of the methanol, ethanol, and ethylene glycol in comparison to the Pt/C is resulted from a combination of the geometric [8], electronic [12], and bifunctional [45] effects. In the first effect, the expansion of Pt–Pt interatomic distance in the PtSb (4.13 Å) and PtSn (4.10 Å) [12] makes it very difficult for carbonaceous species such as CO to bind in bridge site or threefold hollow site configurations [8, 10], inhibiting a possible surface poisoning effect by these species and the consequent decreasing in the electrode performance toward the corresponding reactions. As a second effect, the change in

Table 3 Electrochemical performances of the nanostructured materials in the electro-oxidation of methanol, ethanol, and ethylene glycol by steady-state polarization curves in perchloric acid solution

Catalysts	Organic fuel					
	Methanol		Ethanol		Ethylene glycol	
	j_p (mA.mgPt^{-1})	OP (mV)	j_p (mA.mgPt^{-1})	OP (mV)	j_p (mA.mgPt^{-1})	OP (mV)
Pt/C	20	600	9	600	6	550
PtSn/C	66	450	29	450	27	300
PtSb/C	33	540	19	450	14	440

the electronic density of the surface adsorption sites caused by Sn and Sb in the intermetallics PtSn and PtSb certainly modifies the chemisorption energies for methanol, ethanol, and ethylene glycol on Pt sites. In a recent publication, Pinto and coworkers showed from X-ray photoelectron spectroscopy data that occur a significant variation of the surface electron density distribution of the pure metals involved, when they are combined in 1:1 stoichiometric intermetallics phases PtSn and PtSb. The authors suggest that such changes in electron configuration would certainly promote the alteration of the adsorption energies of all species involved in the process at the catalytic Pt sites and, as a consequence, would make the surface more suitable to oxidize the alcohols and intermediate molecules. Considering the third effect, the presence of the second oxophilic metals in the intermetallic structure promotes the formation of oxygenated species in a potential region less positive than pure platinum, and these species play a crucial role in the oxidation reaction of CO_{ad} directly to CO_2, releasing the actives sites of Pt for further faradaic processes [45, 46]. So far, it is not possible to assure which effect or even which combination of effects is the main responsible for the better performance of the intermetallics toward the alcohol oxidation reactions. However, it was clearly demonstrated that those materials have improved the reactions, and a great deal of study is still demanded to make the processes clearer.

Conclusion

The experimental methodology used in this work to synthesize the supported ordered intermetallic phases of nanoparticles, PtSn and PtSb, has proved to be very effective in producing the intended materials. XRD analysis shows the particles to be crystalline and predominantly made up of the intermetallic phases PtSn and PtSb. TEM images showed that the metal nanoparticles were well dispersed on the carbon support, with a very even distribution and size of these materials in the nanoscale. EDX tests confirmed that the intermetallic phases were of the expected stoichiometry (1:1), demonstrating the efficiency of this method of synthesis. Both these materials were electrocatalytically active for the oxidation of the organic fuels methanol, ethanol, and ethylene glycol. Comparative tests were run with Pt/C prepared by the same method, all the three materials were being used to make ultrathin layer electrodes, and the intermetallics materials electrodes performed best in the electro-oxidation of the fuels in terms of onset potential and current density.

In general, it was concluded that this study has provided valuable insights into the method used to synthesize the ordered intermetallic nanoparticles PtSn/C and PtSb/C, and it has demonstrated the excellent activity of these materials in comparison with Pt/C for the oxidation of alcohols.

Acknowledgments Authors thank FINEP (Proc. 01.06.0939.00) for financial support, and M. R. Silva would like to thank Finep/CNPQ for the scholarship granted (Proc. 380318/2007-5).

References

1. Gonzalez ER (2000) Quim Nova 23:262–266
2. Wendt H, Götz M, Linardi M (2000) Quim Nova 23:538–546
3. Li H, Sun G, Cao L, Jiang L, Xin Q (2007) Electrochim Acta 52:6622–6629
4. Gleiter H (1995) Nanostruct Mater 6:3–14
5. Campelo JM, Luna D, Luque R, Marinas JM, Romero AA (2009) ChemSusChem 2:18–45
6. Sauthoff G (2000) Intermetallics 8:1101–1109
7. Cahn RW (2001) Contemp Phys 42:365–375
8. Zhang L, Xia D (2006) Appl Surf Sci 252:2191–2194
9. Casado-Rivera E, Volpe DJ, Alden L, Lind C, Downie C, Vázquez-Alvarez T, Ângelo ACD, DiSalvo FJ, Abruña HD (2004) J Am Chem Soc 126:4043–4049
10. Casado-Rivera E, Gál Z, Ângelo ACD, Lind C, DiSalvo FJ, Abruña HD (2003) Chem Phys Chem 4:193
11. Blasini DR, Rochefort D, Fachini E, Alden RL, Disalvo FJ, Cabrera CR, Abruña HD (2006) Surf Sci 600:2670–2680
12. Pinto LCM, Silva ER, Caram R, Tremiliosi-Filho G, Ângelo ACD (2008) Intermetallics 16:246–254
13. Innocente AF, Ângelo ACD (2006) J Power Sources 162:151–159
14. Innocente AF, Ângelo ACD (2008) J Power Sources 175:779–783
15. Bauer JC, Chen X, Liu Q, Phan T-H, Schaak RE (2008) J Mater Chem 18:275–282
16. Fievet F, Lagier JP, Blin B, Beaudoin B, Figarez M (1989) Solid State Ionics 198:32–33
17. Joseyphus RJ, Matsumoto T, Takahashi H, Kodama D, Tohji K, Jeyadevan B (2007) J Solid State Chem 180:3008
18. Roychowdhury C, Matsumoto F, Mutolo PF, Abruña HD, DiSalvo FJ (2005) Chem Mater 17:5871–5876
19. Cable RE, Schaak RE (2005) Chem Mater 17:6835–6841
20. Sra AK, Schaak RE (2004) J Am Chem Soc 126:6667–6672
21. Cable RE, Schaak RE (2006) J Am Chem Soc 128:9588–9589
22. Henderson NL, Schaak RE (2008) Chem Mater 20:3212–3217
23. Watanabe M, Uchida M, Motoo S (1987) J Electroanal Chem 229:395–406
24. Liu Z, Guo B, Hong L, Lim TH (2006) Electrochem Commun 8:83–90
25. Neto AO, Dias RR, Tusi MM, Linardi M, Spinacé EV (2007) J Power Sources 166:87–91
26. Guo Y, Zheng Y, Huang M (2008) Electrochim Acta 53:3102–3108
27. Colmati F, Antolini E, Gonzalez ER (2005) Electrochim Acta 50:5496–5503
28. Cullity BD, Stock SR (2001) Elements of X-Ray Diffraction, 3rd edn. Prentice Hall, Upper Saddle River
29. Spinacé EV, Linardi M, Neto AO (2005) Electrochem Commun 7:365
30. Perez J, Gonzalez ER, Ticianelli EA (1998) Electrochim Acta 44:1329
31. Ralph TR, Hogarth MP (2002) Platinum Metals Rev 46:3–14
32. Gurau B, Viswanathan R, Liu R, Lafrenz TJ, Ley KL, Smotkin ES, Reddington E, Sapienza A, Chan BC, Mallouk TE, Sarangapani S (1998) J Phys Chem B 102:9997

33. Iwasita T (2002) Electrochim Acta 47:3663–3674
34. Manohara R, Goodenough JB (1992) J Mater Chem 2:875
35. Oliveira RTS, Santos MC, Marcussi BG, Nascente PAP, Bulhões LOS, Pereira EC (2005) J Electroanal Chem 575:177–182
36. Chen S, Schell M (1999) J Electroanal Chem 478:108–117
37. Lemos SG, Oliveira RTS, Santos MC, Nascente PAP, Bulhões LOS, Pereira EC (2007) J Power Sources 163:695–701
38. Xia XH, Liess HD, Iwasita T (1997) J Electroanal Chem 437:233–240
39. Iwasita T, Pastor EA (1994) Electrochim Acta 39:531–537
40. Camara GA, Iwasita T (2005) J Electroanal Chem 578:315–321
41. Kelaidopoulou A, Abelidou E, Papoutsis A, Polychroniadis EK, Kokkinidis G (1998) J Appl Electrochem 28:1101–1106
42. Wang H, Jusys Z, Behm RJ (2009) Electrochim Acta 54:6484–6498
43. Chatterjee M, Chatterjee A, Ghosh S, Basumallick I (2009) Electrochim Acta 54:7299–7304
44. Salvaraj V, Vinoba M, Alagar M (2008) J Colloid Interface Sci 322:537–544
45. de los Santos-Álvarez N, Alden LR, Rus E, Wang H, DiSalvo FJ, Abruña HD (2009) J Electroanal Chem 626:14–22
46. Lopes PP, Ticianelli EA (2007) Quim Nova 30:1256–1260